Liu *et al.*
Journal of Engineering and Applied Science (2024) 71:90
https://doi.org/10.1186/s44147-024-00423-9

Journal of Engineering and Applied Science

RESEARCH Open Access

Influence of tool nose angle on cutting performance in hot machining of Inconel 718

Xin Liu[1*], Xiaoliang Lin[1], Xiaowei Jia[1], Yueyang Li[1*] and Changfeng Shao[2]

*Correspondence:
848511657@qq.com;
z2013167@sdaeu.edu.cn

[1] College of Mechanical and Electronic Engineering, Shandong Agriculture and Engineering University, Shandong Province, Jinan 250100, People's Republic of China
[2] Jiangsu University, Jiangsu Province, Zhenjiang, People's Republic of China

Abstract

Superalloy Inconel718 is an important material for aircraft preparation because of its excellent performance at high temperatures. However, when cutting Inconel718, a large amount of cutting heat will be generated, resulting in excessive tool temperature and serious wear, which accelerates the tool failure. In order to solve this problem, the influence of tool angle on the process of thermal aided machining was studied by simulation model combined with thermal aided machining technology. During the cutting process, the workpiece preheating temperature rises from room temperature 20° C to 500° C, the front tool angle range is − 5° to 10°, and the rear tool angle range is 4° to 16°. By analyzing various parameters, it was found that a smaller tool rake angle can effectively reduce the tool temperature. Additionally, a flank angle of around 12° was found to decrease the maximum wear area of the tool by approximately 10.5%. Moreover, it was observed that implementing heat-assisted machining can result in a significant reduction of tool temperature by 11.1%, as well as a decrease in cutting force ranging from 18 to 22%, particularly at temperatures exceeding 500 °C.

Keywords: Rake angel, Flank angle, Hot-machining, Inconel 718, Cutting temperature

Introduction

Nickel alloys are extensively utilized in industries such as aerospace and precision machinery due to their exceptional properties. However, the high temperatures generated during the cutting process and the challenging nature of processing these alloys make them difficult and costly to machine. Additionally, these conditions can adversely affect the lifespan of the machining tools.

In recent years, there has been a growing interest among researchers in utilizing heat-assisted machining technology for processing nickel alloys. Several studies have shown that this technology can effectively reduce cutting forces and extend the tool life during the hot working process. Venkatesan et al. [1–3] conducted research on cutting Inconel 718 using laser heat-assisted technology. They found that this approach could reduce cutting forces, minimize tool wear, and improve the surface roughness of the workpiece. They also discovered that a 60° laser heating angle was particularly effective. Moon and Lee [4] employed plasma thermal machining to mill Inconel 718 and AISI1045 workpieces. Their findings revealed that this method could decrease cutting forces and enhance the surface integrity of the workpiece. Tosun and Ozler [5, 6] utilized liquefied petroleum gas as a heat source

to heat the workpiece and cut manganese steel materials. They observed that this technique could improve tool life and reduce the surface roughness of the workpiece. Sofuoğlu M A et al. [7–11] studied the energy consumption factors in thermal-assisted machining of aerospace materials and conducted economic research and optimized the parameters of thermal-assisted machining combined with different simulation software. Parida et al. [12–15] focused on heat-assisted machining of titanium alloys and nickel-based alloys. Their research indicated that this approach could enhance the chip formation process, reduce cutting forces, and decrease the material's resistance to machining strength. They also discovered that increasing the hot working temperature further improved these effects.

Despite the increase in cutting temperature associated with heat-assisted machining, researchers continue to explore its application in processing nickel alloys. To address the issue of high temperatures, studies have investigated ways to reduce cutting temperature through different approaches. One aspect researchers have focused on is the tool nose angle, as it has been found to have a significant impact on cutting temperature. By adjusting the tool nose angle, researchers have discovered that it can improve cutting temperature in both roughing and finishing processes of the material. Qu et al. [16] conducted grinding experiments by varying the rake face angle and found that a larger rake angle on the cutting edge effectively reduces surface roughness, improves surface quality, and decreases grinding force and energy consumption. Azaath et al. [17] studied the effect of rake angle and tool geometry on the machining process of AISI4340. They observed that varying the rake angle altered the chip-tool contact, leading to a reduction in tool wear rate. Saptaji et al. [18] investigated the influence of corner angle and tool nose angle in micro-milling and found that increasing the angle effectively reduced burr formation. Anilchandra et al. [19] found that a negative rake angle facilitated chip breakage and minimized the impact of continuous chips on the machined surface. Liu et al. [20] examined the effect of tool nose angle on cutting Al-based SiC materials and discovered that negative chamfers ensured the integrity of the workpiece surface. This is because the angle of the tool tip influences the direction of force acting on the silicon carbide particles. In summary, there are optimal tool nose angles for machining different materials. Researchers have explored and identified these angles to improve the cutting temperature, quality, and efficiency in various machining processes.

Heat generation in cutting is primarily influenced by plastic deformation and friction, which are directly related to the rake and relief angles of the tool. Furthermore, the volume of the tool tip plays a crucial role in heat transfer. The volume of the tool tip is also associated with the rake and relief angles of the tool. In this study, the focus is on investigating the effects of different nose angles on various parameters in the cutting process, specifically when thermally assisted machining of nickel alloys is employed. The aim is to understand the relationship between the tool angle and parameters such as cutting temperature and cutting force through range analysis, while ensuring the preservation of the advantageous features of thermal-assisted machining technology.

Experimental

Johnson–cook model for Inconel 718

Given that cutting processes can induce significant thermal strains in the material and are conducted under thermally assisted machining conditions, the Johnson–Cook (J-C) model is chosen as the material model in this study. References [21, 22]

Table 1 Chemical composition of the Inconel 718 [23]

Element	Ni	Nb	C	Ti	Cr	Co	Mo	Al	Fe
Percentage	52	5.5	0.08	1.15	21	1.0	3.3	0.7	Balance

Table 2 Physical and mechanical properties of Inconel718 at different temperatures

Property	**Value**	
	Room temperature	**650 °C**
Thermal conductivity (W/m°C)	13.7	22
Specific heat (J/Kg°C)	435	554
Thermal expansion (θ/°C)	1.20×10^{-5}	1.52×10^{-5}
Density (kg/m^3)	8192	-
Poisson ratio	0.3	0.28
Melting point (°C)	1260–1320	-

demonstrate the simulation results with different J–C model parameters, which confirm the reliability of the model. The model utilized in this study is represented by the following equation:

$$\sigma = \left(1290 + 895\varepsilon^{0.526}\right) \times \left(1 + 0.016ln\frac{\overline{\varepsilon}}{0.03}\right) \times \left(1 - \left(\frac{T - T_r}{T_m - T_r}\right)^{1.55}\right)$$

where σ is the flow stress, ε is true strain, $\overline{\varepsilon}$ is true strain-rate, and T, T_{m}, and T_{r} are work, material, and melting and room temperature respectively ($T_{\mathrm{m}} = 1300$ °C, $T_{\mathrm{r}} = 20$ °C).

The chemical composition and thermo-physical properties of Inconel 718 alloy for the cutting test are shown in Tables 1 and 2.

The establishment of the simulation process

The finite element method is employed to analyze heat-assisted processing. In the experimental process, the heating device for the material is depicted in Fig. 1a. Figure 1b illustrates the principle of thermal processing for the material, where a flame torch is used for heating and a temperature detection device monitors the thermal processing temperature.

The geometric configuration and boundary conditions of the finite element simulation model are presented in Fig. 1c. The workpiece model has a height of 0.7 mm and a length of 3 mm. In the simulation experiment, the workpiece material utilized is Inconel 718, and an adaptive meshing method is applied for workpiece meshing. The minimum mesh size is set to 4 μm, and the maximum mesh size is 70 μm. Higher mesh density is employed based on the relative changes between the workpiece and the tool. The total number of elements in the model amounts to 1668.

The bottom of the workpiece is fixed as a boundary condition, with a constant moving speed of 88 m/min in the X direction and fixed in the Y direction. The depth of cut is 0.1 mm, and the tool material is WC cemented carbide with a nose radius of 20 μm.

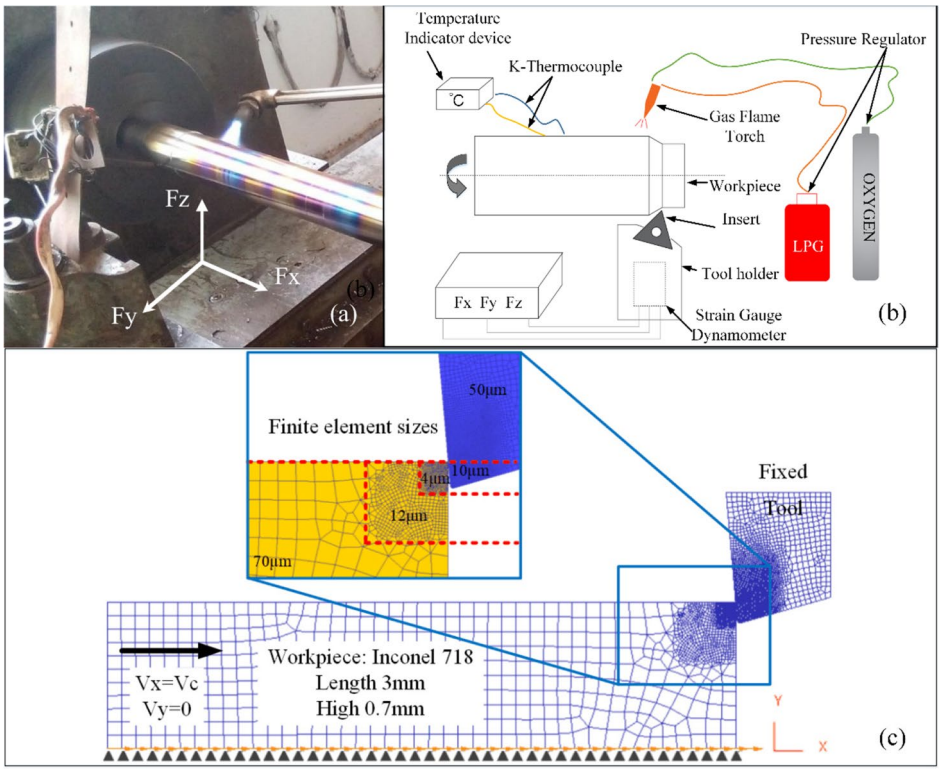

Fig. 1 Hot machining. **a** Experimental setup [24]. **b** Schematic diagram. **c** The boundary and meshing conditions of FE models

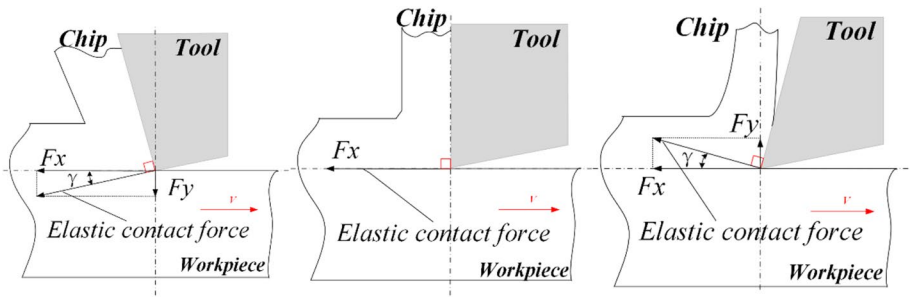

Fig. 2 The state of cutting force components at different nose angles

Angle analysis

The theoretical force model of the rake angle in different states is illustrated in Fig. 2. When the tool rake angle is negative, the material undergoes compression during the cutting process, causing a downward force component on the workpiece material. When the tool is cutting vertically, the force on the material is solely the cutting force in the horizontal direction, with no vertical cutting force acting on it. Conversely, when the tool rake angle is positive, it can be observed that the cutting force on the material is more pronounced, aiding in the separation of the chips from the workpiece. A comprehensive comparison reveals that when the tool rake angle is negative, the cutting force is greater due to the mutual compression of the material between the tool surface and the workpiece. Therefore, when the tool angle is negative, the overall cutting force during the cutting process is greater compared

to the other two conditions. Furthermore, when the rake angle is negative, the compression of the material worsens the heat dissipation conditions during cutting. As a result, the maximum value of the cutting temperature generated during the cutting process theoretically tends to be higher when the tool rake angle is negative compared to the other two conditions.

The influence of the relief angle on the cutting temperature and cutting force is not significant compared with the rake angle, but it will still have different degrees of influence on the quality of the machined surface of the material and the degree of heat dissipation.

Take into account that in the cutting process, the tool geometry angles required for roughing and finishing are different. In this paper, four different rake angles and knife relief angles were selected. And compared with 4 different heat-assisted processing temperatures, the combination is shown in Table 3.

Friction model

The primary source of friction encountered in the cutting process arises from the relative motion that occurs when the cutting tool and the surface of the workpiece come into contact. Accurately predicting and describing the friction behavior between the tool and the workpiece surface is a challenging issue that needs to be addressed in the current field of cutting. Successfully resolving this problem is essential for ensuring the precision of cutting simulation outcomes. In a study conducted by Özel et al. [25], the researchers examined the impact of different friction models on the cutting process. The friction model using the hybrid model is $\tau = \mu k$. The value of μ is shown in Table 4.

Wear model

In this study, the Usui wear model was employed, and the finite element-based tool wear prediction method developed by Yen et al. [26] was utilized in a two-dimensional model. The simulation results obtained using the Usui wear model were compared with experimental data in this paper, and its reliability was confirmed by Malakizadi et al. in their research [27]. The Usui wear model is represented by the following equation.

$$\omega = \int apVe^{-b/T}dt$$

Table 3 Parameters for the cutting simulation

Property	Value
Material	Inconel 718
Cutting tool	Uncoated WC insert
Cutting speed (m/min)	88
Depth of cut (μm)	0.1
Heating temperature (°C)	20, 100, 300, 500
Cutting edge radius (μm)	20
Rake angle (deg)	−5, 0, 5, 10
Clearance angle (deg)	4, 8, 12, 16
Minimum element size (mm)	0.04
Maximum element size (mm)	0.7

Table 4 Friction and wear parameter

Parameters	Value
μ	0.6
a	0.00001
b	1000

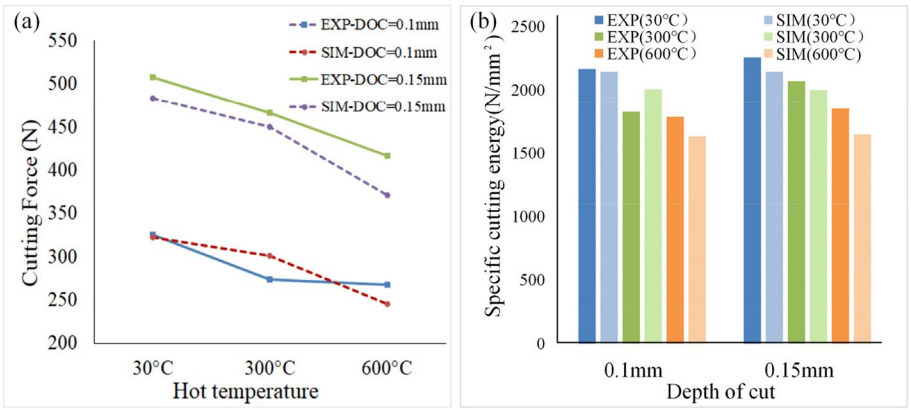

Fig. 3 Comparison of experimental [24] and simulated data. **a** Cutting forces. **b** Specific cutting energy

where p is interface pressure, V is sliding velocity, T is interface temperature, dt is time increment, and a and b are experimentally calibrated coefficients. And a and b are set to 1×10^{-5} and 1000 respectively.

Results and discussion

Simulation and experiment comparison

Figure 3 presents a comparison of cutting forces and specific cutting energy during the cutting of nickel-based alloys under thermally assisted machining conditions. The results indicate a close resemblance between the simulated results obtained using the power exponential J–C model and the experimental data. This result shows the cutting force and specific cutting energy state at different cutting depths (specifically 0.1 mm and 0.15 mm) at a cutting speed of 66 m/min, and the simulation results are very close to the experimental results.

Figure 4 illustrates a comparison between the simulated results obtained using the power function J–C model and the experimental cutting results. In the experiment, the tool had a rake angle of 20°, relief angle of 7°, and a cutting edge with a blunt round radius of 20 μm. The findings indicate a close agreement between the simulation and experimental results, particularly in terms of chip thickness and cutting thickness.

Result data

The cutting simulation is carried out according to the combination scheme given in Table 3, and the cutting parameters are set as fixed values. The cutting speed is 88 m per minute, and the depth of cut is 0.1 mm. Tables 5, 6, 7, and 8 show the resulting data for different tool nose angles at different heat-assisted machining temperatures.

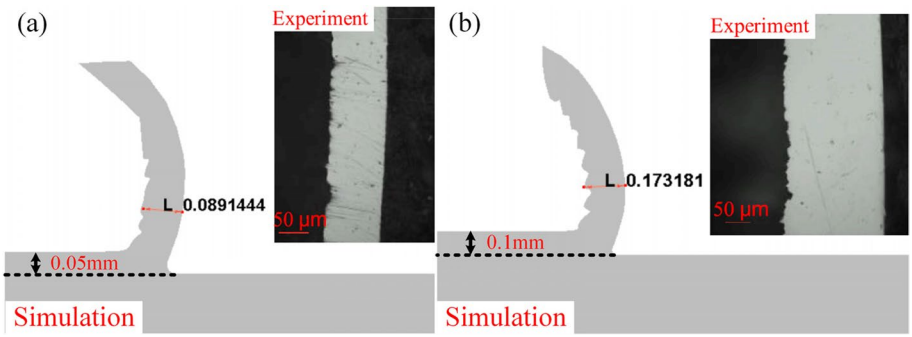

Fig. 4 Simulated and measured [23] chip morphology

Table 5 Cutting data results for different nose angles at 20 °C

No	γ (°)	α (°)	Tool temperature (°C)	Force (N)	Tool wear (10^{-5} mm)
1	−5	4	297	373	619
2	0	4	343	321	712
3	5	4	386	288	660
4	10	4	411	258	745
5	−5	8	283	371	533
6	0	8	344	328	561
7	5	8	383	286	680
8	10	8	426	261	730
9	−5	12	287	370	552
10	0	12	345	324	573
11	5	12	398	291	661
12	10	12	439	255	619
13	−5	16	297	372	579
14	0	16	355	318	737
15	5	16	408	288	710
16	10	16	452	263	657

In this paper, the temperature change, cutting force, and wear state caused by tool angle change in the cutting process are analyzed.

Cutting temperature

In the cutting process, the cutting temperature plays a crucial role in determining the quality of the cut, while the temperature of the tool itself affects tool wear and service life. Figure 5 displays the temperature distribution variations across the rake angle during thermally assisted machining. Under different heat-assisted machining temperature conditions, it is observed that both the maximum cutting temperature and the high-temperature range decrease as the rake angle increases. This implies that as the rake angle increases, the extrusion effect of the tool on the workpiece material decreases, leading to an expanded temperature diffusion area and subsequently reducing the cutting temperature. Additionally, as the rake angle increases, the chip shape transitions from a continuous shape to a sawtooth shape. However, once the heat-assisted processing temperature surpasses 500 °C, the chip shape remains continuous without further changes,

Table 6 Cutting data results for different nose angles at 100 °C

No	γ (°)	α (°)	Tool temperature (°C)	Force (N)	Tool wear (10^{-5} mm)
1	−5	4	278	353	528
2	0	4	354	318	764
3	5	4	384	282	699
4	10	4	424	259	788
5	−5	8	281	348	519
6	0	8	353	322	742
7	5	8	387	281	707
8	10	8	430	256	736
9	−5	12	287	352	534
10	0	12	342	319	597
11	5	12	408	282	701
12	10	12	442	257	655
13	−5	16	302	351	608
14	0	16	368	320	760
15	5	16	412	283	747
16	10	16	447	255	678

Table 7 Cutting data results for different nose angles at 300 °C

No	γ (°)	α (°)	Tool temperature (°C)	Force (N)	Tool wear (10^{-5} mm)
1	−5	4	279	309	688
2	0	4	298	291	606
3	5	4	375	275	618
4	10	4	411	248	829
5	−5	8	284	310	570
6	0	8	310	290	498
7	5	8	373	274	685
8	10	8	421	247	754
9	−5	12	292	310	583
10	0	12	318	290	525
11	5	12	364	277	615
12	10	12	442	247	715
13	−5	16	303	307	627
14	0	16	327	292	619
15	5	16	403	277	682
16	10	16	447	247	724

presumably due to the softening of the workpiece material at higher temperatures, eliminating serration. Furthermore, it can be noted that as the thermally assisted machining temperature increases, the influence of the tool nose angle on the cutting temperature gradually diminishes. Nevertheless, increasing the rake angle still contributes to lowering the maximum cutting temperature.

While the influence of the flank angle on the cutting temperature may not be readily apparent, it does have a considerable impact on the temperature distribution within the machined workpiece. Figure 6 displays the temperature distribution of the machined

Table 8 Cutting data results for different nose angles at 500 °C

No	γ (°)	α (°)	Tool temperature (°C)	Force (N)	Tool wear (10^{-5} mm)
1	−5	4	284	268	761
2	0	4	306	252	690
3	5	4	332	237	609
4	10	4	361	220	622
5	−5	8	286	269	632
6	0	8	313	252	543
7	5	8	337	237	642
8	10	8	372	219	589
9	−5	12	293	267	669
10	0	12	321	253	602
11	5	12	349	236	566
12	10	12	382	220	547
13	−5	16	303	269	673
14	0	16	327	254	719
15	5	16	355	234	649
16	10	16	393	219	541

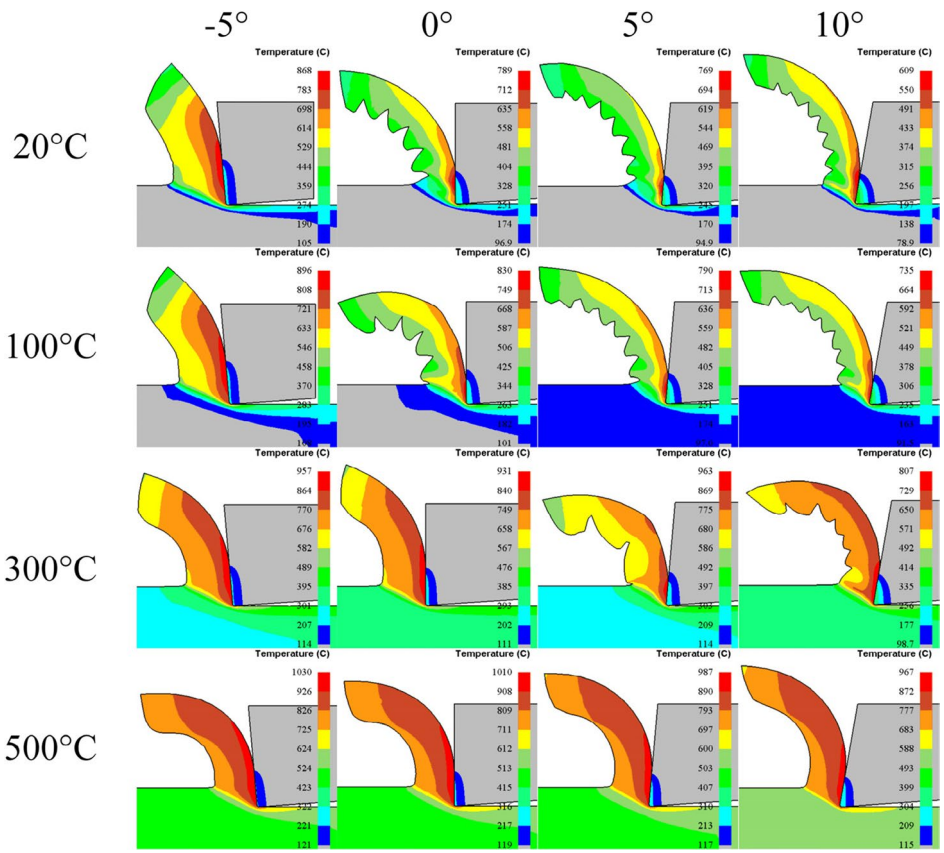

Fig. 5 Temperature distribution for different nose angles and heat assist temperatures (relief angle = 4°)

workpiece for various flank angles. It is observed that as the flank angle increases, the range of the high-temperature area within the machined part gradually diminishes. This can be attributed to the fact that a smaller flank angle results in greater surface extrusion, thereby generating more frictional heat and facilitating a higher rate of temperature diffusion.

Table 9 demonstrates that regardless of the thermally assisted machining temperature conditions employed, the change in rake angle has a more pronounced effect on the temperature of the heated tool compared to the change in flank angle. Furthermore, apart from the optimal tool angle choice of a rake angle of 5° and relief angle of 8° at room temperature, the optimal tool angle selection under other thermally assisted machining temperature conditions is a rake angle of 5° and relief angle of 4°. At room temperature, there is a temperature difference of 0.25 °C between the relief angle of 4° and relief angle of 8°. Consequently, the lowest tool temperature solution is achieved with a rake angle of 5° and relief angle of 4°. This is owing to the fact that an excessively large tool nose angle results in a smaller tool volume, causing the same amount of heat to be concentrated within a smaller volume, leading to elevated temperatures. Conversely, a tool angle that is too small allows for wider temperature dispersion within the tool, thereby reducing the average tool temperature.

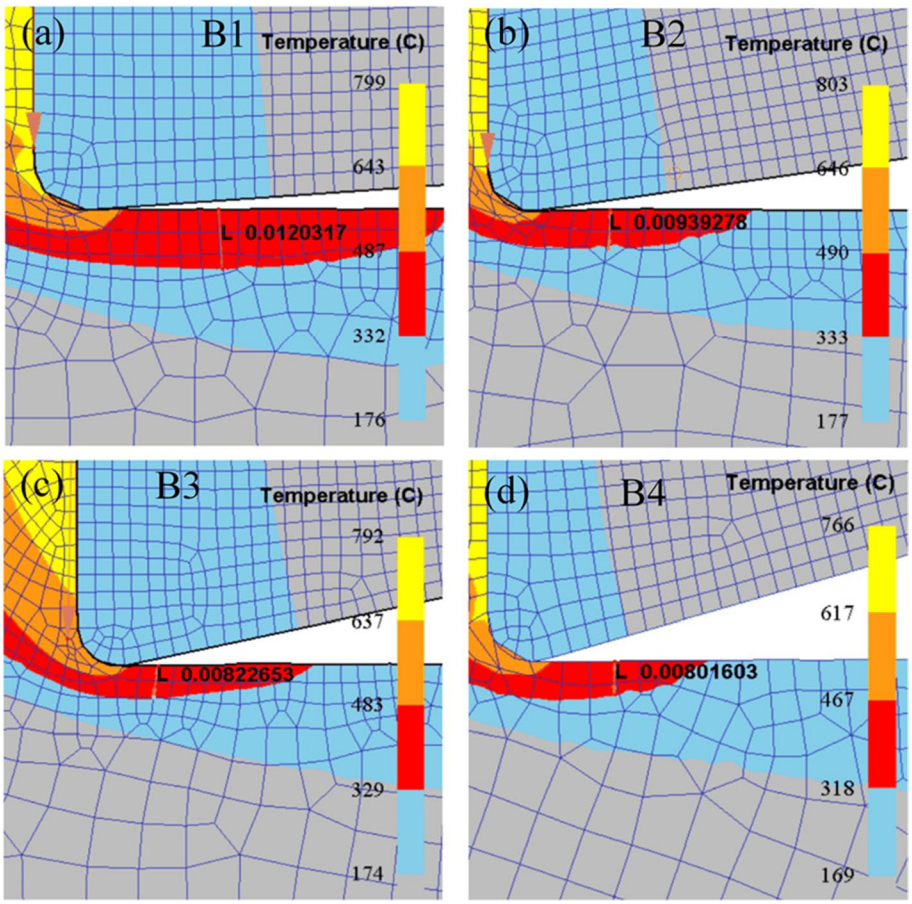

Fig. 6 Temperature distribution of machined surface at different relief angles (rake angle = 0°)

Table 9 Temperature range analysis table

Tool tem	K_{im}	20 °C		100 °C		300 °C		500 °C	
		γ (°)	α (°)	γ (°)	α (°)	γ (°)	α (°)	γ (°)	α (°)
T (°C)	K_{i1}	291	359.25	287	360	289.5	340.75	291.5	320.75
	K_{i2}	346.75	359	354.25	362.75	313.25	347	316.75	327
	K_{i3}	393.75	367.25	397.75	369.75	378.75	354	343.25	336.25
	K_{i4}	432	378	435.75	382.25	430.25	370	377	344.5
	Range	141	19	148.75	22.25	140.75	29.25	85.5	23.75

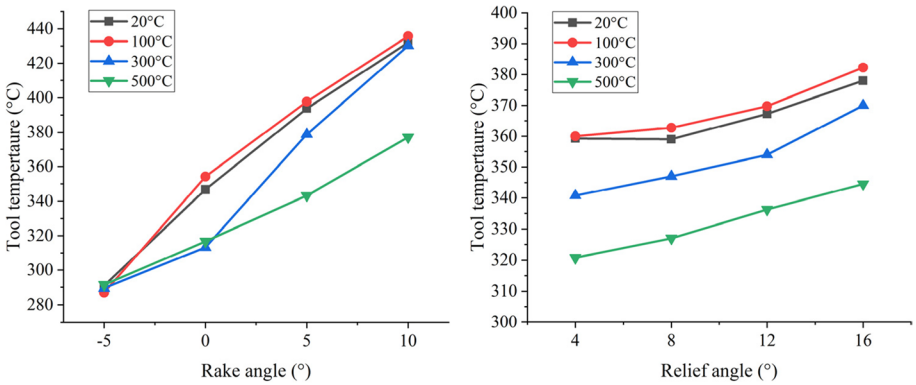

Fig. 7 Average tool temperature at different nose angles

Figure 7 illustrates the variation in average tool temperature as the tool angle changes. It is evident that as both the rake angle and flank angle increase, the tool temperature also rises. This phenomenon arises because, while increasing the rake angle can reduce the heat generated from cutting, it also reduces the volume of the tool tip and consequently hampers heat dissipation. Thus, an excessively large rake angle fails to effectively lower the tool tip temperature. Notably, at heat-assisted machining temperatures of 300 °C and 500 °C, the tool temperature is notably lower compared to other heat-assisted temperatures. This implies that an increase in heat-assisted machining temperature can contribute to a certain extent in reducing tool temperature.

Cutting force

The cutting force is another important parameter in the cutting process, and its magnitude is related to tool life. Figure 8 reveals that the cutting force gradually decreases with an increase in rake angle, in line with the previous analysis of tool angle. Meanwhile, when the rake angle is negative, the cutting force increases due to material extrusion between the tool surface and the workpiece. As the rake angle increases, less material is extruded, resulting in a corresponding reduction in cutting force. On the other hand, the change in flank angle does not significantly affect the cutting force. Notably, at thermally assisted machining temperatures of 300 °C and 500 °C, the cutting force is significantly reduced. This observation correlates with the decrease in tool temperature as the thermally assisted machining temperature increases. Figure 9 illustrates the heat transfer states under different contact conditions. When the cutting force is substantial, as

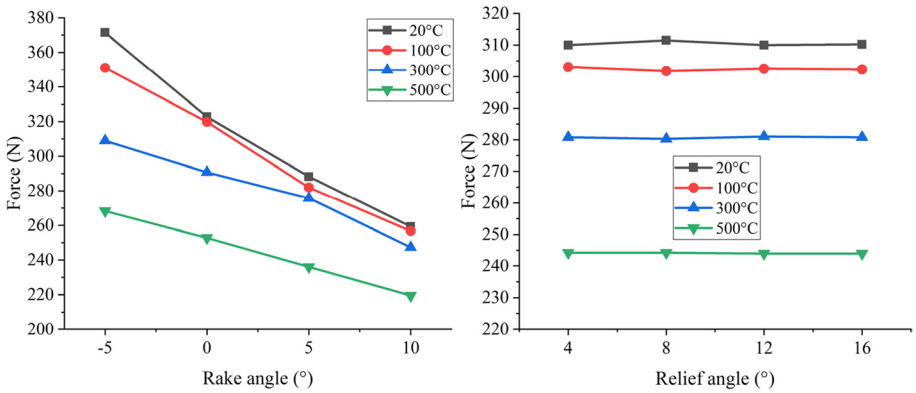

Fig. 8 Average cutting force at different nose angles

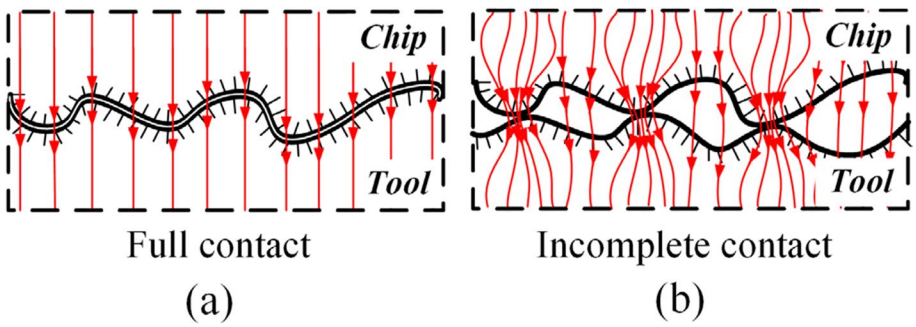

Fig. 9 Heat transfer in different contact states

shown in Fig. 9a, the tool and the chip are in complete contact, facilitating significant heat transfer. However, as the cutting force decreases, the contact force between the tool surface and the chip diminishes, creating a larger gap as depicted in Fig. 9b. This gap accelerates the transfer of cutting temperature to the air, thereby reducing the temperature transferred to the tool.

Wear

The change in tool angle, particularly the rake angle, has a significant impact on the chip flow state. Figure 10 depicts the cutting process, wherein some materials tend to flow slowly or even stagnate near the tool tip's corner, resulting in the formation of a built-up edge known as the dead metal zone (DMZ) [28]. The presence of the DMZ enhances the strength of the cutting edge near it, but it also increases the cutting force. Notably, as shown in Fig. 10, the DMZ is located at the upper part of the tool nose angle [29], and its position does not vary significantly with changes in the thermally assisted machining temperature. This phenomenon has been demonstrated in previous studies as well [30]. Figure 11 illustrates that the minimum wear depth of the tool is situated near the DMZ, while the deepest wear area is near the flank face. As a result, changes in the tool rake angle have no noteworthy effect on the deepest wear area of the tool. However, according to Table 10, increasing the heat-assisted machining temperature helps reduce the deepest wear depth when choosing a larger rake angle.

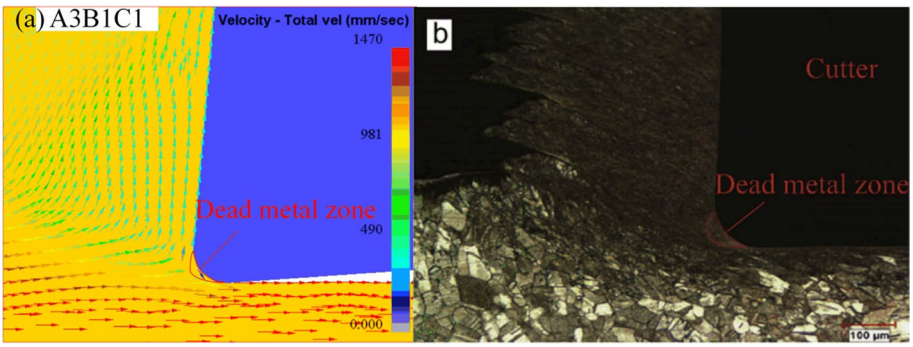

Fig. 10 The position of dead metal zone. **a** Simulation. **b** Experimental [24]

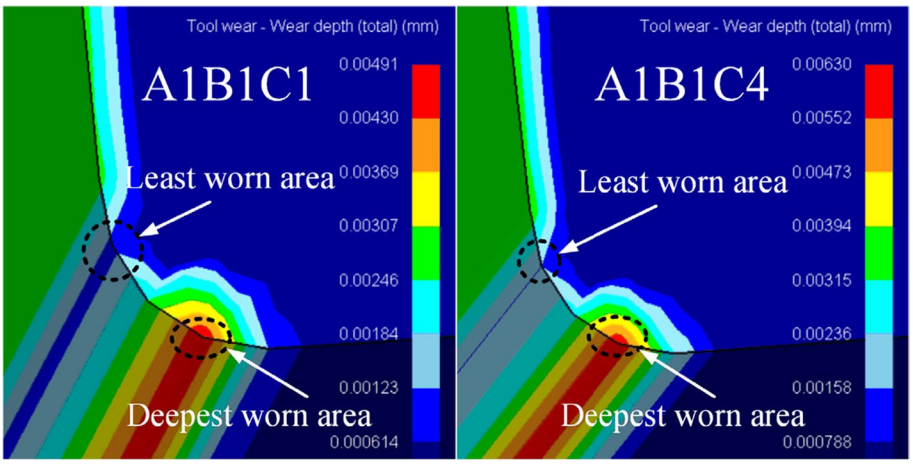

Fig. 11 Tool wear status

Table 10 Wear range analysis table

Wear	K_{im}	20 °C		100 °C		300 °C		500 °C	
		γ (°)	α (°)	γ (°)	α (°)	γ (°)	α (°)	γ (°)	α (°)
W (10^{-5} mm)	K_{i1}	570.75	684	547.25	694.75	617	685.25	683.75	670.5
	K_{i2}	645.75	626	715.75	676	562	626.75	638.5	601.5
	K_{i3}	677.75	601.25	713.5	621.75	650	609.5	616.5	596
	K_{i4}	687.75	670.75	714.25	698.25	755.5	663	574.75	645.5
	Range	117	82.75	168.5	76.5	193.5	75.75	109	74.5

Figure 12 indicates that the smallest deepest wear value is observed when the flank angle is set at 8° and 12°. Therefore, a suitable flank angle falls within the range of approximately 8°–12°. At a heat-assisted machining temperature of 100 °C, the wear depth is higher compared to that at room temperature. This can be attributed to the increased cutting temperature resulting from elevated heat-assisted temperature. However, the cutting force does not decrease significantly, leading to an increased tool wear rate. On the other hand, at a heat-assisted machining temperature of 500 °C,

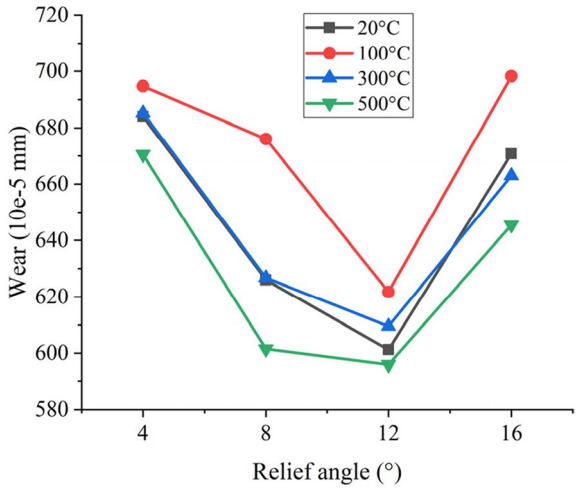

Fig. 12 Average tool wear at different relief angles

the wear depth is notably reduced. This reduction can be attributed to the decrease in cutting force, which leads to reduced heat transfer from the chip to the tool, resulting in decreased friction force and subsequent reduction in tool wear.

Conclusions

Through the establishment of a simulation model for the cutting process of Inconel 718, a difficult-to-machine material, and the investigation and analysis of the influence of cutting process parameters, the following conclusions can be drawn:

1. The tool angle exhibits a positive correlation with tool temperature. A smaller tool nose angle can effectively reduce the tool temperature, but it may result in an increase in cutting temperature. When roughing materials that can withstand high temperatures, a smaller tool nose angle can be chosen. When finishing, it can be paired with a larger tool nose angle and a thermally assisted processing temperature above 300 °C. This approach ensures processing accuracy while reducing tool temperature.
2. The change in flank angle does not have a significant effect on cutting force. Cutting force decreases as the rake angle increases. Increasing the heat-assisted processing temperature can effectively reduce cutting force, with a reduction of 10.8% at 300 °C and 22% at 500 °C.
3. The smallest wear depth under different heat-assisted processing temperatures is observed when the flank angle is approximately 8°–12°. To minimize tool wear, a flank angle of about 8°–12° is recommended.
4. When machining Inconel 718, it is essential to consider tool temperature, cutting force, and tool wear comprehensively. Selecting a rake angle of 5°–10°, a flank angle of 8°–12°, and a heat-assisted processing temperature of 300 °C or higher can effectively improve the cutting conditions and prolong tool life.

Abbreviations

DMZ	Dead metal zone
J-C model	Johnson-Cook model

Acknowledgements
Thanks to Professor Zhicheng Zhang and Professor Xiaofei Cheng for their suggestions on the revision of the article, so as to make the content of the article more abundant and standardized.

Authors' contributions
Xiaoliang Lin and Xiaowei Jia analyzed and verified the usability and accuracy of the model. Xin Liu modeled the tool and analyzed the performance comparison of different texture tools and the effect of texture on the tool. All authors read and approved the final manuscript. Yueyang Li and Changfeng Shao contributed to the content structure and language polishing of the article.

Funding
This work is supported by the Youth Fund of Shandong Agriculture and Engineering University (QNKJZ202301).

Availability of data and materials
The material and data in this paper are obtained by software simulation and quoting other people's experimental data.

Declarations

Ethical approval and consent to participate
The research field of this article is the field of machining and does not involve any ethical issues (not applicable).

Consent for publication
All authors agree to contribute and publish articles. And the data of others in this article have been copyrighted.

Competing interests
The authors declare that they have no competing interests.

Received: 19 February 2024 Accepted: 30 March 2024
Published online: 12 April 2024

References

1. Venkatesan K, Ramanujam R, Kuppan P (2016) Parametric modeling and optimization of laser scanning parameters during laser assisted machining of Inconel 718. Opt Laser Technol 78:10–18
2. Venkatesan K, Ramanujam R (2016) Optimisation of machining parameters in laser aided hybrid machining of Inconel 718. Int J Mach Mach Mater 18(3):252–272
3. Venkatesan K, Ramanujam R, Kuppan P (2017) Investigation of machinability characteristics and chip morphology study in laser-assisted machining of Inconel 718. Int J Adv Manuf Technol 91:3807–3821
4. Moon S-H, Lee C-M (2018) A study on the machining characteristics using plasma assisted machining of AISI 1045 steel and Inconel 718. Int J Mech Sci 142–143:595–602
5. Tosun N, Ozler L (2004) Optimisation for hot turning operations with multiple performance characteristics. The International Journal of Advanced Manufacturing Technology 23(11–12):777–782
6. Tosun N, Özler L (2002) A study of tool life in hot machining using artificial neural networks and regression analysis method. J Mater Process Technol 124(1–2):99–104
7. Gürgen S, Sofuoğlu MA (2021) Advancements in conventional machining: a case of vibration and heat-assisted machining of aerospace alloys[M]. Advanced Machining and Finishing. Elsevier 2021:143–175
8. Sofuoğlu MA, Kushan MC, Orak S (2019) Comparison of different FEM software in terms of hot ultrasonic assisted machining technique[C] Materials Science Forum. Trans Tech Publications Ltd 972:203–207
9. Sofuoğlu M, Gürgen S, Çakir F et al (2019) Design and Economic Analysis of a Novel Hot Ultrasonic Machining System. JOURNAL OF POLYTECHNIC- Politeknik Dergisi 22(2):277–282. https://doi.org/10.2339/politeknik.523697
10. Sofuoğlu MA, Kuşhan MC, Sezan O (2021) Hot ultrasonic assisted machining modelling of Ti6Al4V in terms of power consumption. Journal of Advances in Manufacturing Engineering 2(2):33–41
11. Sofuoğlu MA, Çakır FH, Kuşhan MC et al (2019) Optimization of different non-traditional turning processes using soft computing methods. Soft Comput 23:5213–5231
12. Parida, AK, Maity K (2018) Numerical analysis of chip geometry on hot machining of nickel base alloy. Journal of the Brazilian Society of Mechanical Sciences and Engineering 40(10):498. https://doi.org/10.1007/s40430-018-1418-8
13. Parida AK, Maity K (2020) FEM and experimental analysis of thermal assisted machining of titanium base alloys. Measurement 152:107292
14. Parida AK, Maity K (2019) Hot machining of Ti–6Al–4V: FE analysis and experimental validation. Sådhanå 44:142. https://doi.org/10.1007/s12046-019-1127-8
15. Parida AK (2018) Simulation and experimental investigation of drilling of Ti-6Al-4V alloy. International Journal of Lightweight Materials and Manufacture 1:197–205
16. Qu M et al (2020) Design of binderless grinding wheel with positive rake angle and fabrication used femtosecond laser ablation for grinding soft and brittle crystals. Opt Lasers Eng 124:105803
17. Azaath LM, Mohan E, Natarajan U (2021) Effect of rake angle and tool geometry during machining process of AISI 4340 steel in finite element approach. Materials Today: Proceedings 37:3731–3736

18. Saptaji K, Subbiah S, Dhupia JS (2012) Effect of side edge angle and effective rake angle on top burrs in micro-milling. Precis Eng 36:444–450
19. Anilchandra AR, Surappa MK (2010) Influence of tool rake angle on the quality of pure magnesium chip-consolidated product. J Mater Process Technol 210:423–428
20. Liu HZ, Wang SJ, Zong WJ (2019) Tool rake angle selection in micro-machining of 45 vol.%SiCp/2024Al based on its brittle-plastic properties. J Manuf Process 37:556–562. https://doi.org/10.1016/j.jmapro.2018.12.030
21. Laakso SVA, Niemi E (2017) Using FEM simulations of cutting for evaluating the performance of different johnson cook parameter sets acquired with inverse methods. Robotics and Computer-Integrated Manufacturing 47:95–101
22. Bikash CB, Sudarsan G, Venkateswara R (2018) Modeling of cutting force in MQL machining environment considering chip tool contact friction. Tribol Int 117:283–295
23. Tian P et al (2022) Reverse identification of constitutive parameters of Inconel 718 alloy based on analytical model and thermo-mechanical loads analysis of machined surface. Journal o f materials research and technology 16:1353–1370
24. Parida, AK, Maity K (2018) Numerical and Experimental Analysis of Specific Cutting Energy in Hot Turning of Inconel 718. Measurement 133:361–369
25. Olleak A, Zel T (2017) 3D Finite Element Modeling Based Investigations of Micro-textured Tool Designs in Machining Titanium Alloy Ti-6Al-4V. Procedia Manuf 10:536–545. https://doi.org/10.1016/j.promfg.2017.07.042
26. Yen YC, Lilly B, Altan T (2004) Estimation of tool wear in orthogonal cutting using the finite element analysis. J Mater Process Technol 146:82–91
27. Malakizadi A, Gruber H, Sadik I, Nyborg L (2016) An FEM-based approach for tool wear estimation in machining. Wear 368–369:10–24
28. Rao KV, Babu BH, Prasad VUV (2019) A study on effect of dead metal zone on tool vibration, cutting and thrust forces in micro milling of Inconel 718. J Alloy Compd 793:343–351
29. Min W, DanYang W, YingChao M, WeiHong Z (2019) On material separation and cutting force prediction in micro milling through involving the effect of dead metal zone. Int J Mach Tools Manuf 146:103452
30. Xin L, Xu Z, Dazhong W (2020) Numerical analysis of different cutting edge radii in hot micro-cutting of Inconel 718. Proc I Mech E, Part C: J Mech Eng Sci. 234:196–210

Publisher's Note